Role of the geodesic acoustic mode shearing feedback loop in transport bifurcations and turbulence spreading

K. Miki and P. H. Diamond
Center for Astrophysics and Space Science, University of California, San Diego, California 92093, USA

(Received 15 September 2009; accepted 11 February 2010; published online 18 March 2010)

A theory of the effect of the geodesic acoustic mode (GAM) on turbulence is presented. Two synergistic issues are elucidated: namely, the physics of the zonal flow modulation and its role in the L-H transition, and the role of the GAM wave group propagation in turbulence spreading. Using a wavekinetic modulational analysis, the response of the turbulence intensity field to the GAM is calculated. This analysis differs from previous studies of zero-frequency zonal flows since it accounts for resonance between the drift wave group speed and the GAM strain field, which induces secularity. This mechanism is referred to as secular stochastic shearing. Finite real frequency and radial group velocity are intrinsic to the GAM, so its propagation can induce nonlocal phenomena at the edge and pedestal regions. To understand the effect of the GAM on turbulence and transition dynamics, a predator-prey model incorporating the dynamics of both turbulence and the GAMs is constructed and analyzed for stability around fixed points. Three possible states are identified, namely, an L-modelike stationary state, a reduced turbulence state, and a GAM limit-cycle state. The system is attracted to the state with the minimum turbulence level. © *2010 American Institute of Physics*. [doi:10.1063/1.3353037]

I. INTRODUCTION

Zonal flows (ZFs), which are poloidal $\mathbf{E}\times\mathbf{B}$ plasma flows due to toroidally and poloidally symmetric $(m=n=0)$ potential perturbations and the accompanying coherent shearing poloidal flows, have attracted significant attention.[1] Since the discovery of the undamped residue of the ZF,[2] the geodesic acoustic mode (GAM),[3] which is an oscillatory counterpart of ZF, coupled to an up-down-asymmetric pressure perturbation with $(m,n)=(1,0)$, has also been received attention as a possible mechanism for regulation of turbulent transport. The GAM is weakly damped by Landau resonance, but is sometimes more easily excited by the Reynolds stress drive than the zero-frequency ZF (ZFZF) residue. The GAM damping tends to be of order $\exp(-q^2)$, so that the GAM is weakly damped in regions with higher safety factor. In the edge region, the coherence time of shearing increases. It also produces no secondary transport in itself, because it has $n=0$. Research has uncovered that tokamak ZFs are composed of two kinds of eigenmodes with having specific frequencies, namely, high-frequency ZFs (HFZFs) and low-frequency or ZFZFs. The HFZFs are the GAM oscillations, which are damped by ion Landau resonance (for $\omega_{\mathrm{LD}}\sim k_{\parallel}v_{\mathrm{ti}}$). The low-frequency/ZFZFs are, in turn, damped by collisions on a longer time scale. Hence, we see that different types of damping and shearing dynamics can coexist in the ZFs.

Concerning turbulence regulation by the GAMs, there indeed are experimental results indicating some link between changes in turbulent fluctuation levels and the GAMs.[4–7] Reference 5 suggests that the GAMs are related to L-H transition dynamics. In experiments on edge turbulence in DIII-D involving variation in applied neutral beam power, torque and the consequent toroidal plasma rotation, the poloidal turbulence velocity spectrum exhibits a transition from a GAM frequency to a lower-frequency, zero-mean-frequency ZF, as rotation varies from cocurrent to balanced, thus facilitating the L-H transition. Here the GAM possibly is a player in the L-H transition dynamics, because it is easily excited in region of high safety factor $q(r)$, i.e., especially in the edge region. Thus, it is useful to build a model for describing the transition accompanied by GAM shearing so as to estimate turbulent transport in the edge region at high safety factor $q(r)$.

In this work, we discuss the theory of GAM effects on turbulence and transition dynamics, based on a simple shearing model. Two key issues are discussed. First, due to its finite frequency, a qualitatively different shearing modulation of the GAMs is distinguished from that for ZFZFs. In particular, *secular stochastic shearing* can result from the resonance between group velocity of the drift-wave packet and GAM phase velocity, whereas the phase velocity of the ZFZFs is necessarily zero, so broadening must be considered for irreversibility. The resonance enables coherent shearing by the oscillatory GAM field.

Second, GAM group propagation, which is induced by ion polarization screening effects, causes a nonlocal contribution to turbulence and also radiative dissipation induced by the Doppler shift in the GAM frequency. Since the GAM frequency depends on radial wave number q_r, its group velocity $v_{\mathrm{gr,GAM}}=\partial\omega/\partial q_r$ is thus defined, and propagation in a bounded medium causes radiative dissipation of the GAM energy. Radially coherent GAM eigenmodes, with a certain typical scale length and corresponding propagation toward the edge, can also be described using the Airy function.[8] The consequent radial propagation can couple core with edge, and can also promote the propagation of turbulence, i.e., turbulence spreading,[9,10] as shown in Fig. 1. The GAM group propagation is an intrinsically different mechanism from that

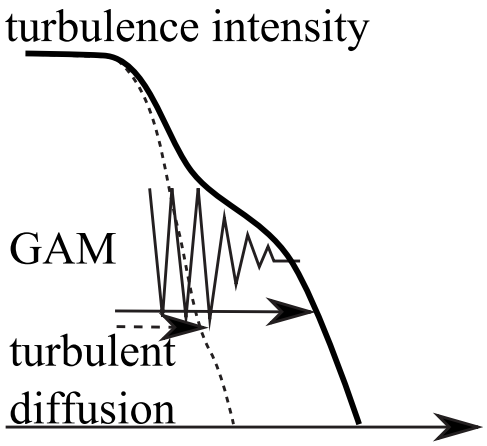

FIG. 1. Illustration of the effect of GAM propagation on turbulence spreading. The dotted line shows the profile of turbulent intensity with only turbulent diffusion. The bold line shows the consequent profile of turbulent intensity also with GAM propagation.

that caused by nonlinear turbulence self-diffusion. We discuss the scale length of the GAM propagation as compared with the GAM damping length.

The radiative dissipation due to the GAM group propagation causes an effective correction to the GAM frequency, which we refer to as the radiative Doppler shift in the GAM frequency. Because the GAM frequency must be constant along the propagation trajectory, the observed frequency in a particular fixed radial location can be expanded when the phase velocity and the group velocity are in the opposite direction. We discuss the calculation of the radiative dissipation of the GAM and corresponding effect on the change in time scale of the GAMs.

To semiquantitatively understand turbulence transport dynamics in the presence of GAM shearing, we construct a model based of the well-known predator-prey type.[11] We identify possible states of the system by using stability analyses around the fixed points. Here we identify three types of states, an L-modelike steady state, a reduced turbulence state, and an oscillatory state, which we identify as the GAM state. The stability analysis tells us which state is actually selected. The outcome can be deduced from a diagram in the space of the growth rate of turbulence and the Landau damping rate of the GAM. From this figure, we can recover a transition from the L-modelike steady state to the oscillatory state by increasing the heating power. We also obtain the effective GAM frequency explicitly, including the effect of radiative dissipation.

The remainder of this paper is organized as follows. In Sec. II, we discuss the impact of the GAMs on turbulence and classify the basic interaction mechanisms. One is secular stochastic shearing by the GAMs and the others are the effects of propagation and radiative dissipation. In Sec. III, we present a L-H transition model describing the predator-prey relation between turbulence and the GAMs. In Sec. IV, we discuss the significance of the results of this work.

II. PHYSICS OF GAM-TURBULENCE INTERACTION

In this section, we discuss the impact of the GAMs on turbulence by considering two physics mechanisms, namely: (i) shearing effects and (ii) propagation of GAMs. ZFs are also generated by turbulence through the shearing-tilting process. However because of the finite real frequency of GAMs, more care is required in the treatment of HFZF (GAM) shearing dynamics, a feature not emphasized by previous works concerning GAM dynamics. The other effect enters via the finite group velocity of the GAMs. Therefore, HFZFs may propagate and induce nonlocal phenomena or radiative damping.

A. Shearing model

Based on the wavekinetic equation,[12] we obtain the time evolution for the *mean* wave action density as

$$\frac{\partial\langle N\rangle}{\partial t} = \frac{\partial}{\partial k_r} D \frac{\partial\langle N\rangle}{\partial k_r}, \tag{1}$$

where $N=\varepsilon/\omega_k$ is wave action density, ε is turbulence energy, $\omega_k = k_\theta V_*/(1+k_\perp^2\rho_i^2)$ is drift frequency, (for the drift wave mode $\mathbf{k}$), k_r and k_θ are the radial and poloidal wave numbers of turbulence fluctuation respectively, $V_* = c_s\omega_{ci}^{-1}L_n^{-1}$ is diamagnetic velocity and the diffusion coefficient D (for scattering in k_r) can be written as

$$D = \sum_{q_r} q_r^2 k_\theta^2 |\tilde{V}_q|^2 \pi\delta[\Omega_q - q_r V_{\rm gr}(k)], \tag{2}$$

where q_r is the radial wave number of the GAMs, $\tilde{V}_q$ is the amplitude of oscillatory $\mathbf{E}\times\mathbf{B}$ poloidal flow velocity, Ω_q is the finite real frequency of the GAMs, (Ω_q is negligible in the case of ZFZFs), and $V_{\rm gr}$ is the group velocity of drift wave packet. D can be calculated by using autocorrelation time scale $\tau_{\rm ac}$ taking into account three wave resonance between GAM and turbulence. Here

$$D \simeq \int_q q^2 k_\theta^2 |\tilde{V}_q|^2 \tau_{{\rm ac},\omega,\underline{k}}, \tag{3}$$

where

$$\tau_{{\rm ac},\omega,\underline{k}} \sim |(v_{\rm gr,GAM} - v_{\rm ph,GAM})\Delta q|^{-1}, \tag{4}$$

is the autocorrelation time for a drift wave-packet interaction with the GAM shearing field. $\tau_{\rm ac}$ measures the coherence of the drift wave packet with the GAM shearing field. Δq is the width of the envelope of the GAM packet in radial wave number. Notice that $v_{\rm gr,DW}=v_{\rm ph,GAM}$ at resonance.

Multiplying ω_k by Eq. (1) and integrating, we obtain

$$\frac{\partial\langle\varepsilon\rangle}{\partial t} = -\int d\underline{k} \frac{d\omega_k}{dk_r} D \frac{\partial\langle N\rangle}{\partial k_r}, \tag{5}$$

which is an evolution equation for the DW energy due to GAM interaction. Then,

$$\frac{\partial\langle\varepsilon\rangle}{\partial t} \simeq -\int \mathrm{d}\underline{k} v_{\mathrm{gr}}(k_r)\sum_q q^2 k_\theta^2 |\tilde{V}_q|^2 \tau_{\mathrm{ac}} \frac{\partial\langle N\rangle}{\partial k}$$

$$\simeq +\int \mathrm{d}\underline{k} \frac{2\rho_i^2 k_r}{(1+k_\perp^2\rho_i^2)^2}\sum_q q^2 k_\theta^2 |\tilde{V}_q|^2 \tau_{\mathrm{ac}} \frac{\partial\Omega}{\partial k_r}, \quad (6)$$

where Ω is the potential enstrophy density of turbulence, proportional, but not equal to the drift wave energy. Assuming $\mathrm{d}\Omega/\mathrm{d}k_r<0$ (i.e., the turbulence spectrum always decays at small scale), we proceed as

$$\frac{\mathrm{d}\langle\varepsilon\rangle}{\mathrm{d}t} = -\int \mathrm{d}\underline{k} \frac{2\rho_i^2 k_\theta^2}{(1+k_\perp^2\rho_i^2)}\sum_q q^2 |\tilde{V}_q|^2 \tau_{\mathrm{ac}} \langle\varepsilon_k\rangle \sigma, \quad (7)$$

where $\langle\varepsilon_k\rangle$ is mean turbulence energy of the drift wave with wave number k, and $\sigma=-(k_r\partial\Omega/\partial k_r)/\Omega$ is characteristic of the slope in wave number of the drift wave spectrum. Now we refer to σ as a spectral index, so we obtain the averaged wave energy damping rate as

$$\gamma_{\mathrm{DW}} = \frac{1}{\langle\varepsilon\rangle}\frac{\mathrm{d}\langle\varepsilon\rangle}{\mathrm{d}t}$$

$$= -\frac{1}{\langle\varepsilon\rangle}\int \mathrm{d}\underline{k} \frac{2\rho_i^2 k_\theta^2}{(1+k_\perp^2\rho_i^2)}\sum_q q^2 |\tilde{V}_q|^2 \tau_{\mathrm{ac}} \sigma \langle\varepsilon_k\rangle. \quad (8)$$

Finally, we derive the following time evolution of turbulence energy as a response to $\mathbf{E}\times\mathbf{B}$ shear $|V'|$, DW-GAM coherence τ_{ac}, and turbulence energy ε

$$\frac{\partial\langle\varepsilon\rangle}{\partial t} \sim -2\sigma\langle k_\theta^2\rho_i^2/(1+k_\perp^2\rho_i^2)\rangle\langle\varepsilon\rangle|\tilde{V}'|^2\tau_{\mathrm{ac}} \sim -|V'|^2\tau_{\mathrm{ac}}\langle\varepsilon\rangle. \quad (9)$$

This formulation is similar to that used in the predator-prey model for the interplay between turbulence and (zero-frequency) ZF,[13] but involves a different coefficient of ZF modulation.

An issue for the GAM shearing theory here is that the wave-packet GAM τ_{ac} is both qualitatively and quantitatively different from its counterpart for the ZFZF. This is due to the finite GAM frequency Ω_q. While $\tau_{\mathrm{ac,ZF}}$ includes a nonlinear decay time of the ZFs, $\tau_{\mathrm{ac,GAM}}$ accounts for packet dispersion, and allows secular GAM shearing at finite frequency. Note also that moderate GAM dispersion ensures that τ_{ac} will be significantly larger than $|v_{\mathrm{ph,GAM}}\Delta q|^{-1}$. Furthermore, the autocorrelation time scale of the GAM, $\tau_{\mathrm{ac,GAM}}$ is definitely lower than that in the case of ZFZFs, $\tau_{\mathrm{ac,ZFZF}}$, as $\tau_{\mathrm{ac,GAM}}>\tau_{\mathrm{ac,ZFZF}}=[v_{\mathrm{gr,DW}}\Delta q]^{-1}$. This is because $v_{\mathrm{gr,DW}}\propto -v_*$, so the time scale of DW-ZF correlation is comparatively short. Thus, by energy conservation, the production of the GAM must also be reduced, as compared with DW time scales. It is useful to discuss how much we can estimate the time scale ratio. Recalling $V_{\mathrm{gr,DW}}\sim v_*\sim v_{\mathrm{ti}}/L_n$, where v_* is ion diamagnetic velocity, $v_{\mathrm{ti}}=\sqrt{T_i/m_i}$ is the ion thermal velocity, and L_n is the characteristic length of density profile, $\omega_{\mathrm{GAM}}\sim v_{\mathrm{ti}}/R$, and also q_r is the order of $1/\rho_i$ in the ITG turbulence,[14] we can estimate the ratio of the GAM production rate to that of ZFZF as

$$\frac{\alpha_{\mathrm{ZFZF}}}{\alpha_{\mathrm{GAM}}} \sim \frac{\tau_{\mathrm{ZFZF}}}{\tau_{\mathrm{GAM}}} \sim \frac{\omega_{\mathrm{GAM}}/q_r + V_{\mathrm{gr,DW}}}{V_{\mathrm{gr,DW}}}$$

$$\sim L_n/R + 1 \sim 1 + a/R. \quad (10)$$

Therefore, we find that the relative impact on turbulence of the zero and finite frequency ZF depend upon the inverse aspect ratio.

Note that this result is superficially similar to the result of Ref. 15, in that the reduction in $\mathbf{E}\times\mathbf{B}$ shearing rate due to finite frequency is determined by the ratio of the real frequency to the autocorrelation rate of the turbulence. However our result improves upon that of Ref. 15, because it properly treats GAM wave-packet structure and because the two-point correlation analysis in Ref. 15 artificially presumes a particular GAM time variation, and does not account for the correlation time's dependence on the turbulence spectrum. In particular, we note that GAM dispersion is crucial to determining τ_{ac}.

B. GAM propagation

In this subsection, we discuss the effect of the GAM group propagation on turbulence, and especially on nonlocal effects. Including the finite Larmor radius (FLR) effect, the dispersion relation of the GAM is simply described as

$$(1+q_r^2\rho_i^2)\omega_{\mathrm{GAM}}^2 = \omega_{\mathrm{GAM},0}^2, \quad (11)$$

where q_r is the GAM radial wave number, ω_{GAM} is the GAM frequency with finite ρ_i and $\omega_{\mathrm{GAM},0}$ is the GAM frequency in the limit of no FLR effect, i.e., $\rho_i \ll 1$. The bracket on the left-hand side in Eq. (11) is characteristic of FLR corrections to the ion pressure. $\omega_{\mathrm{GAM},0}$ is stated as $\omega_{\mathrm{GAM},0}=\sqrt{2\Gamma}(c_s/R)$ in the case with finite ion temperature and cold electron, where c_s is the ion sound speed and $\Gamma=5/3$ is the ratio of specific heats.

For stationary ZF, the group velocity vanishes because the ZF has zero real frequency. Therefore the dynamics of ZFs can be treated as local. Any wave-packet propagation will necessarily drag the ZF along. However, the GAMs have a dispersive real frequency, so they can propagate radially. The GAM group propagation velocity $v_{\mathrm{gr,GAM}}$ is

$$v_{\mathrm{gr,GAM}} \simeq \frac{\partial}{\partial q_r}\left(\frac{\omega_{\mathrm{GAM},0}}{(1+q_r^2\rho_i^2)^{1/2}}\right) = -\frac{\omega_{\mathrm{GAM},0}q_r\rho_i^2}{(1+q_r^2\rho_i^2)^{3/2}}. \quad (12)$$

The lifetime of the GAM packet is the reciprocal of the Landau damping rate γ_{LD}, i.e., $\tau_{\mathrm{LD}}=1/\gamma_{\mathrm{LD}}$. Therefore the scale length of the GAM propagation, or the typical scale length for GAM nonlocality, can be estimated to be

$$(\Delta x)_{\mathrm{GAM}} \sim v_{\mathrm{gr,GAM}}\tau_{\mathrm{LD}} = \frac{\omega_{\mathrm{GAM},0}}{\gamma_{\mathrm{LD}}}\frac{q_r\rho_i^2}{(1+q_r^2\rho_i^2)^{3/2}}. \quad (13)$$

Equation (13) shows that the scale length of the GAM packet penetration is the order of $\rho_i\omega_{\mathrm{GAM},0}/\gamma_{\mathrm{LD}}$, so a high $q(r)$ configuration leads to considerable radial synchronization, because γ_{LD} is small in high safety factor regions. Note this in effect defines a new edge (and pedestal) length scale.

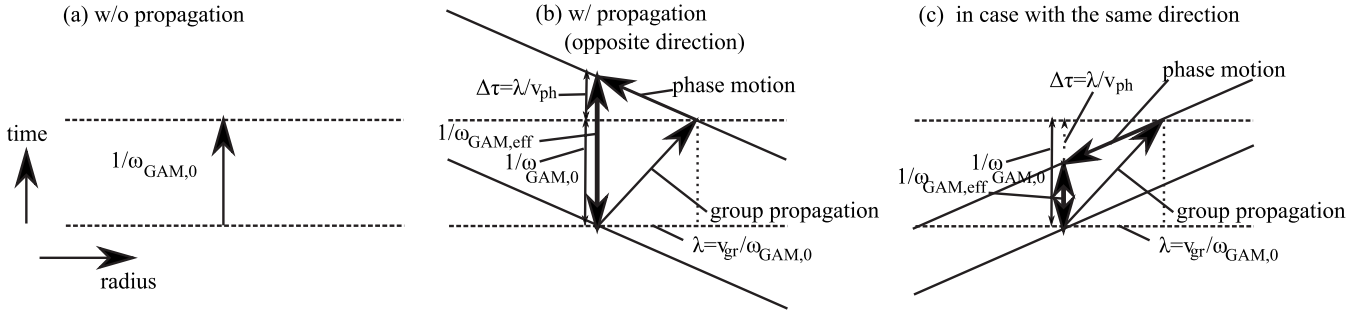

FIG. 2. Illustration of the GAM propagation and modulation of the GAM frequency as a diagram in the space of radius and time. (a) Without GAM propagation, the wave propagates only vertically (without variation in the radial direction), while (b) with the GAM propagation, due to radial motion, the time scale of the GAM oscillation is expanded by $\Delta\tau=\lambda/v_{ph}$. (c) shows the case when the direction of GAM phase and group velocities are the same.

Another scale length governing the nonlocal dynamics is that of turbulence spreading, $(\Delta x)_{TS}\sim\sqrt{D/\gamma_z}$,[16] where D is the parameter for the nonlinear spatial diffusion and γ_z is the damping rate of turbulence in the stable region. It is found that GAM propagation should be taken into account in nonlocal dynamics such as turbulence spreading, when $(\Delta x)_{GAM}$ is comparable to $(\Delta x)_{TS}$. The situation is expected when the safety factor $q(r)$ is high enough in the edge region.

The effect of the radiative dissipation of the GAM can be understood systematically as a kind of Doppler shift by illustrating GAM propagation, as in Fig. 2. Here the horizontal direction indicates radial variation and the vertical shows time evolution. Now we take the directions of the group and the phase velocities to be opposite, i.e., $v_{gr}v_{ph}<0$, as is shown in Landau-fluid simulations[17] and is also clear from the dispersion relation. As seen in Fig. 2, in the case of normal oscillation without spatial GAM propagation, the trajectory evolves in vertical direction only, indicating evolution in time alone, so that the scale of the oscillation τ is just the reciprocal to the GAM frequency, $\tau=1/\omega_{GAM}$. In turn, if dependence of the GAM frequency on q_r is now introduced, the GAM phase speed $v_{ph}=\omega_{GAM}/q_r$ and the group speed $v_{gr}=\partial\omega/\partial q_r$ appear. Suppose a GAM packet propagates on the GAM time scale $1/\omega_{GAM}$ at the group speed v_{gr}. The centroid position moves by $\lambda=|v_{gr}|/\omega_{GAM}$. This is, then, the scale length for GAM propagation.

Now the effective time scale of the GAM $1/\omega_{GAM,eff}$ is seen to increase by $\Delta\tau$ due to the effective Doppler shift induced by group propagation, i.e., $1/\omega_{GAM,eff}=1/\omega_{GAM}+\Delta\tau$. The difference $\Delta\tau$ is obtained by dividing the scale length of the GAM propagation by the phase speed v_{ph}, $\Delta\tau=\lambda/v_{ph}=|v_{gr}|/(\omega_{GAM}v_{ph})$. See Fig. 2(b). Thus, we obtain the following relation:

$$\frac{1}{\omega_{GAM,eff}}=\frac{1}{\omega_{GAM,0}}\left(1+\frac{|v_{gr}|}{v_{ph}}\right). \tag{14}$$

Finally we get a differential equation,

$$\omega_{GAM,eff}=\omega_{GAM}-q_r\left|\frac{\partial\omega_{GAM,eff}}{\partial q_r}\right|. \tag{15}$$

This is a radiative Doppler effect due to the GAM group propagation. Note that the actual calculation involves the effect of the Landau damping via λ. As we discussed above, the scale length for the GAM's spillover into the stable region inevitably depends on the GAM propagation dynamics. To solve for the effective GAM frequency, we need take into account the effect of Landau damping. We will solve for it using a simplified model.

Note that assuming the same sign for the GAM group and phase velocity, $v_{GAM,gr}v_{GAM,ph}>0$, we obtain that the effective GAM frequency is increased by the ratio of $v_{GAM,gr}$ to $v_{GAM,ph}$. This is because the effective GAM time is reduced by the recession in time by the phase velocity of the GAM, as shown in Fig. 2(c).

III. SIMPLIFIED MODEL WITH CLOSED FEEDBACK LOOP

Here we describe a novel predator-prey model in terms of the turbulence fluctuation and the GAMs. The minimum model for describing the GAM-turbulence interaction is based on that discussed in Refs. 18 and 19, neglecting the anisotropic parallel perturbation, assuming a high-q configuration.

A. Derivation of the equations of zonal flow and anisotropic pressure perturbation

Starting from the predator-prey model formulated in terms of the turbulence and ZF (N,U), we first expand the model to describe the interplay between the turbulence and the GAM shearing, by including a new degree of freedom, i.e., the anisotropic pressure perturbation. Here we will discuss a leakage of perpendicular current due to grad B drift, which is the so-called geodesic curvature.[3]

From $\nabla\cdot J=0$, the time evolution of the vorticity can be written as

$$-\frac{ne}{B\omega_{ci}}\left(\frac{\partial}{\partial t}+v_E\cdot\nabla\right)\nabla_\perp^2\phi-\frac{2}{B_0R_0}[x,(p_i+p_e)]=0, \tag{16}$$

where $v_E\equiv\mathbf{E}\times\mathbf{B}/B^2$ is $\mathbf{E}\times\mathbf{B}$ drift and p_i and p_e are the ion and electron pressure perturbations, respectively. Here the first term corresponds to the divergence of ion polarization drift, the second term does the divergence of ion and electron diamagnetic drift, employing the radial variation in $B\propto 1/(1+r/R\cos\theta)$ as the toroidal coordinate, and the parallel dissipation of current is neglected since electrons are Boltzmann. The importance is that leakage of current due to

the grad B drifts occurs in toroidal geometry, and contributes to generation of the GAM.

Applying the following normalization:

$$(tv_{ti}/a, r/\rho_i, \rho_i\nabla_\perp, a\nabla_\parallel) \to (t, r, \nabla_\perp, \nabla_\parallel),$$
$$\frac{a}{\rho_i}\left(\frac{n}{n_c}, \frac{e\phi}{T_c}, \frac{v_\parallel}{v_{ti}}, \frac{p_i}{p_c}\right) \to (n, \phi, v_\parallel, p_i), \tag{17}$$

we obtain the normalized form of the vorticity equation

$$\left(\frac{\partial}{\partial t} + v_E \cdot \nabla\right)\nabla_\perp^2 \phi = -\frac{2a}{R}[x, (p_i + p_e)]. \tag{18}$$

Taking a flux surface average $\langle\cdot\rangle \equiv \int d\theta d\zeta$, we obtain the equation in terms of ZF potential $\Phi_0 \equiv \langle\phi\rangle$.

$$\frac{\partial}{\partial t}\nabla_\perp^2 \Phi_0 = \langle[\tilde{\phi}, \nabla_\perp^2 \tilde{\phi}]\rangle - \frac{2a}{R}\langle[x, p]\rangle, \tag{19}$$

where p is total pressure written by $p \equiv p_i + p_e$. Now we obtain the equation for the ZF velocity $U \equiv \nabla\Phi_0$ as follows:

$$\frac{\partial U}{\partial t} = -\left\langle \frac{\partial\tilde{\phi}}{\partial\theta}\nabla_\perp^2\tilde{\phi}\right\rangle - \frac{2a}{R}\langle p \sin\theta\rangle. \tag{20}$$

The first term is the vorticity flux, and so the Reynolds stress drive, driven by the turbulence fluctuations. The second term is the geodesic curvature term connecting with $p(1,0)$ anisotropic pressure perturbation, thus generating the GAM. Making the *ansatz* $\Phi_0 \sim \Phi_q \exp(+iq_r r)$ and also $U \sim iq_r\Phi_q$, and assuming that $q \ll \Delta k_r$, where Δk_r denotes the width of the drift wave spectrum in k_r, the Reynolds stress term can be written in terms of q_r as

$$-\left\langle \frac{\partial\tilde{\phi}}{\partial\theta}\nabla_\perp^2\tilde{\phi}\right\rangle = -\sum_{\mathbf{k}_1+\mathbf{k}_2=\mathbf{q}} k_{1\theta}k_{2\perp}^2\tilde{\phi}_{\mathbf{k}_1}\tilde{\phi}_{\mathbf{k}_2}. \tag{21}$$

Note that we here use k normalized by ρ_i. Neglecting noise from drift waves, using $\mathcal{E}_\mathbf{k} = (1+k_\perp^2)|\phi_\mathbf{k}|^2$ and applying a quasilinear wavekinetic treatment,[20] we obtain the energy density relation

$$\text{RHS of Eq.(21)} = -q_r^2\sum_\mathbf{k}\frac{\omega_{*e}k_\theta k_r}{(1+k_\perp^2)}R(\Omega,k,q)\frac{\partial\langle\Omega\rangle}{\partial k_r}U_q, \tag{22}$$

where the response function

$$R(\Omega,k,q) = \frac{|\gamma_k|}{(\Omega - qV_{gr})^2 + \gamma_k^2} \tag{23}$$

is related to the autocorrelation time of the GAM $\tau_{ac,GAM}$. Here we include the finite real frequency in the GAM shearing effect. Note that the factor which multiplies U_q in Eq. (22) is the familiar ZF growth rate, now modified to include finite GAM frequency.

For the anisotropic pressure perturbation $\langle p \sin\theta\rangle$, the time evolution is described[21] as

$$\frac{\partial}{\partial t}\langle p \sin\theta\rangle = (\Gamma+\tau)p_{eq}\frac{a}{R}\langle v_{E_r}\rangle - (\Gamma-1) \times\sqrt{\frac{8T_{eq}}{\pi}}\frac{a}{qR}\langle T_i \sin\theta\rangle - v_{gr,GAM}\nabla_r\langle p \sin\theta\rangle, \tag{24}$$

where n_{eq} and p_{eq} and T_{eq} are the density, ion pressure, and ion temperature equilibrium profile quantities normalized to their values at the core, respectively. Here the pressure nonlinearity is caused by $\mathbf{E}\times\mathbf{B}$ drift convection $\langle[\phi,p]\sin\theta\rangle$. Also, we note that (2,0) contributions, density/temperature gradient source terms, temperature relaxation contribution, and any coupling term between $\langle v_{E_r}\rangle$ and $\langle p\cos\theta\rangle$ are neglected. Here we also neglect the contribution of $\langle v_\parallel \cos\theta\rangle$, assuming high safety factor $q(r)$. Now we introduce a term reproducing the group propagation of the GAM as the third term in the right-hand side (r.h.s.) of Eq. (24), which is

$$\left(\frac{\partial}{\partial t} + v_E\nabla\right) \to \left(\frac{\partial}{\partial t} + (v_E + v_{gr,GAM})\nabla\right). \tag{25}$$

Note that the effect of the radiative Doppler dissipation is relevant only in the case that the system is oscillatory, since $v_{gr,GAM} \propto \omega_{GAM}$.

B. analysis of model

The dynamics of the DW-GAM system are more easily grasped by considering a zero-dimensional model, instead of the one-dimensional model. The GAM model based on three fields (U,G,V) involves both zero-frequency and high-frequency eigenmodes.[18] However, the relation between turbulence and the mixture of ZF and GAM shearing, which is the mixture of zero-frequency and HFZFs, is still uncertain. Nonetheless, we can construct a model limited to high-frequency components, which neglects the contribution of the anisotropic parallel velocity $\langle v_\parallel \cos\theta\rangle$, in order to avoid the complexity of frequency mixing in the shearing model. This assumption is valid for high safety factor $q(r)$ values.

Thus, we regard the following as two "predators:" HFZF velocity $U \equiv \langle v_{E_r}\rangle$, and $G = \langle p \sin\theta\rangle$, the up-down asymmetric ion pressure perturbation. The "prey" is the turbulence N. The evolution of these components is described by

$$\frac{\partial N}{\partial t} = \gamma_L N - \Delta\omega N^2 - \alpha' U^2 N, \tag{26a}$$

$$\frac{\partial U}{\partial t} = (1/2)\alpha' UN - \beta G - v_{gr,GAM}\nabla_r U, \tag{26b}$$

$$\frac{\partial G}{\partial t} = \beta' U - \gamma_{LD} G - v_{gr,GAM}\nabla_r G. \tag{26c}$$

Here γ_L is the growth rate of the turbulence energy, which may be estimated from the result of simulation or experiments by using $\gamma_L = \gamma_0(\kappa - \kappa_c)$, where κ is observed ion temperature gradient, κ_c corresponds to the linear critical temperature gradient, and γ_0 is a reference growth rate. In order that the turbulence fluctuations are unstable, $\kappa > \kappa_c$

is required. $\Delta\omega$ is the nonlinear damping rate of the turbulence, α' is the ZF modulation rate discussed before, which is the order of $q_r^2\tau_{ac,GAM}$. Also, $\beta=2(a/R)/n_{eq}$, $\beta'=(5/3)\times(a/R)p_{eq}/(1+q_r^2)$, where q_r is radial wave number of the GAMs normalized by $1/\rho_i$. Here we add the factor $1/(1+q_r^2)$ as the screening effect by the ion polarization drift. Note that the terms associated with β and β' corresponds to the geodesic curvature, so the basic time scale of the GAM frequency is defined as $\omega_{GAM}^2=\omega_{GAM,0}^2/(1+q_r^2)=\beta\beta'=(5/3)\times(a/R)^2T_{eq}/(1+q_r^2)$. Here $\omega_{GAM,0}$ is the reference frequency in the limit of $q_r\to 0$, which is equivalent to the limit without FLR effects. Here we neglect the electron pressure contribution, characterized by $\tau=T_e/T_i$, for simplicity. In Eqs. (26b) and (26c), we include the terms related to the GAM group propagation $v_{gr,GAM}$. Note that this is effective only when the system is oscillatory, i.e., in a limit-cycle state.

First, we should classify possible solutions of the model. Then we will investigate the stability around each of the fixed points to understand the comprehensive behavior of the solution trajectories for the system.[19,22] Note that the group propagation terms vanish in the limit of a stable state, hence we neglect the radiative dissipation terms in the stability analysis. We expand Eqs. (26a)–(26c) around a fixed point (N_0,U_0,G_0), which is defined as $\partial_t(N_0,U_0,G_0)=0$, for small perturbations $(N_0+\delta N,U_0+\delta U,G_0+\delta G)$. Then the following linear formula involving the dynamical evolution matrix can be written as

$$\frac{\partial}{\partial t}\begin{pmatrix}\delta N\\ \delta U\\ \delta G\end{pmatrix}=\begin{pmatrix}\Delta & -2\alpha' U_0N_0 & 0\\ (1/2)\alpha' U_0 & (1/2)\alpha' N_0 & -\beta\\ 0 & \beta' & -\gamma_{LD}\end{pmatrix}\begin{pmatrix}\delta N\\ \delta U\\ \delta G\end{pmatrix}, \tag{27a}$$

$$\Delta=\gamma_L-2\Delta\omega N_0-\alpha' U_0^2, \tag{27b}$$

where we assume that the small perturbations have eigenvalues λ, i.e., $\delta N\propto\exp(\lambda t)$, $\delta U\propto\exp(\lambda t)$, and $\delta G\propto\exp(\lambda t)$. λ is obtained by finding roots of the eigenequation for the determinant of the dynamical matrix in the r.h.s. of Eq. (27a). For each kind of fixed point, λ can be obtained individually by estimating the stability around the point in the phase space (N,U,G). In the case that all eigenvalues are negative or neutral, and structural stability is thus identified. The fixed points in this model are (i) the trivial one $(N_0,U_0,G_0)=(0,0,0)$, (ii) the L-modelike one $(N_L,0,0)$, and (iii) the reduced turbulence one (N_H,U_H,G_H), where

$$N_L=\frac{\gamma_L}{\Delta\omega}, \tag{28a}$$

$$N_H=\frac{2\omega_{GAM}^2}{\alpha'\gamma_{LD}}, \tag{28b}$$

$$U_H^2=\frac{\Delta\omega}{\alpha'}\left(\frac{\gamma_L}{\Delta\omega}-\frac{2\omega_{GAM}^2}{\alpha'\gamma_{LD}}\right)=\frac{\Delta\omega}{\alpha'}(N_L-N_H), \tag{28c}$$

$$G_H=\frac{\beta'}{\gamma_{LD}}U_H. \tag{28d}$$

Here we investigate the stability about each fixed point. In the case of (i) (0,0,0), which is the trivial solution, the eigenvalues calculated are $\lambda=\gamma_L,-\gamma_{LD}/2\pm i\omega$. The condition for stability is $\gamma_L<0$ and $\gamma_{LD}>0$. The condition $\gamma_L<0$ is not valid in the relevant regime of turbulence excitation, $(\Delta\omega,\alpha',\gamma_L,\gamma_{LD}>0)$, so that the trivial solution is not structurally stable, but rather is a saddle node.

In the case of (ii), L-modelike solution $(N_L,0,0)$, the eigenequation from the determinant of the dynamical matrix is

$$F(\lambda)=(\lambda+\gamma_L)\left[\lambda^2+\left(\gamma_{LD}-\frac{\alpha'\gamma_L}{2\Delta\omega}\right)\lambda+\left(-\frac{\alpha'\gamma_L\gamma_{LD}}{2\Delta\omega}+\omega_{GAM}^2\right)\right]=0. \tag{29}$$

In order that all real components of the eigenvalues are negative, $\gamma_L>0$ and $\gamma_{LD,eff}-(\alpha' N_L)/2>0$ are necessary. If $\gamma_L>0$ is assumed, this condition is equivalent to $N_*-N_L>0$, where $N_*\equiv 2\gamma_{LD,eff}/\alpha'$ is the turbulence level sustained by oscillating predators (U and G) within a limit-cycle orbit, as discussed later.

In the case of (iii) reduced turbulence solution (N_H,U_H,G_H), the equation for the eigenvalues is

$$\begin{aligned}F(\lambda)&=\lambda[\lambda+\Delta\omega N_H]\left[\lambda+\frac{\alpha'}{2}(N_*-N_H)\right]\\&\quad+\alpha'\Delta\omega\gamma_{LD}N_H(N_L-N_H)\\&=\lambda^3+\frac{\alpha'}{2}\left[N_*-\left(1-\frac{2\Delta\omega}{\alpha'}\right)N_H\right]\lambda^2\\&\quad+\frac{\alpha'}{2}\Delta\omega N_H(N_*-N_H)\lambda\\&\quad+\frac{\alpha'^2}{2}\Delta\omega N_*N_H(N_L-N_H)=0.\end{aligned} \tag{30}$$

In order that all real components of the roots in Eq. (30) are negative, the following conditions are required:

$$N_*-N_H>0, \tag{31a}$$

$$N_L-N_H>0. \tag{31b}$$

In other words, the required condition is that N_H is the minimum of N_L, N_H, and N_*. Now we consider the case where both fixed points are not structurally unstable, which is equivalent to the case where N_* is the lowest value in N_L, N_H, and N_*. In this case, the solution with the limit-cycle orbit may be regarded as one of asymptotic stability.

Assuming $N=N_*$, the following quantity C is found to be constant in time along the trajectory of propagation:

$$\left(\frac{\partial}{\partial t}+v_{gr,GAM}\frac{\partial}{\partial r}\right)C=0, \tag{32a}$$

where

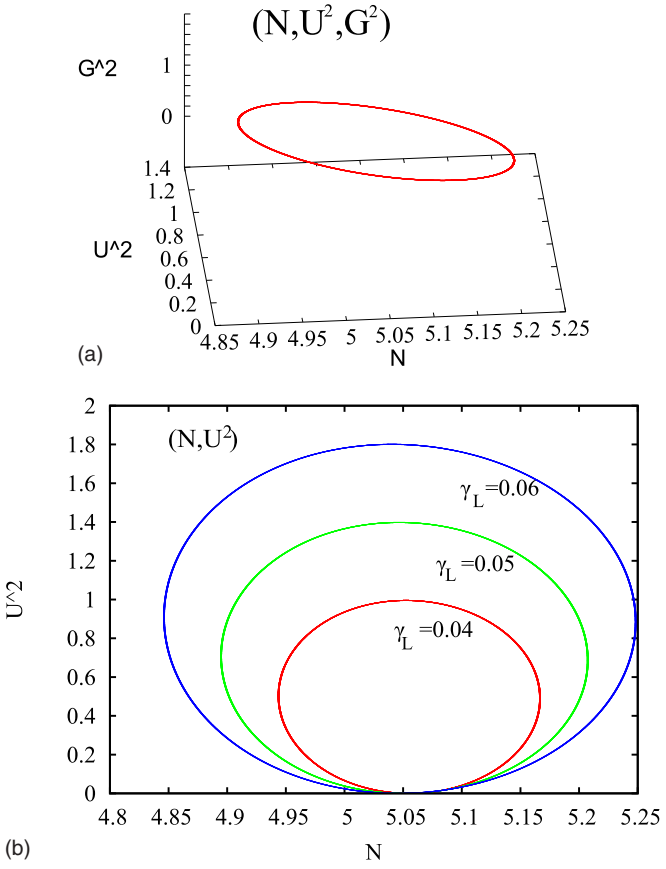

FIG. 3. (Color online) (a) phase portrait in (N,U^2,G^2) and (b) phase portrait in the projection to (N,U^2) with various γ_L=0.04–0.06 in the case of the limit cycle oscillation around $N=N_*\simeq 5.06$.

$$C=\frac{2\beta'}{\alpha' N}U^2+\frac{\beta}{\gamma_{\mathrm{LD}}}G^2-2UG. \tag{32b}$$

This corresponds to an elliptical orbit in the phase portrait of (U,G), as shown in Fig. 3. As seen in Fig. 3(a), the full solution trajectory traces a circular motion around $N=N_*$. Figure 3(b) shows the projection to the space (N,U^2), indicating that the radius in the direction of U^2 is linear in γ_L. Now we estimate how the width of the orbit of U^2 depends on the input heating power via γ_L. Based on insight from the numerical calculation, assuming

$$N=n_0+n_2\exp(-2\mathrm{i}\omega t)+(\mathrm{c.c.}), \tag{33a}$$

$$U=u_1\exp(-\mathrm{i}\omega t+\mathrm{i}q_r r)+(\mathrm{c.c.}), \tag{33b}$$

$$G=g_1\exp(-\mathrm{i}\omega t+\mathrm{i}q_r r)+(\mathrm{c.c.}), \tag{33c}$$

and substituting into Eqs. (26a)–(26c), we obtain

$$0=\gamma_L n_0-\Delta\omega(n_0^2+2n_2n_2^*)-\alpha'(2n_0|u_1|^2+n_2u_1^{*2}+n_2^*u_1^2), \tag{34a}$$

$$-2\mathrm{i}\omega n_2=\gamma_L n_2-2\Delta\omega n_0n_2-\alpha'(2n_2|u_1|^2+n_0u_1^2), \tag{34b}$$

$$-\mathrm{i}\omega u_1=\frac{\alpha'}{2}(u_1n_0+u_1^*n_2)-\beta g_1-\mathrm{i}q_r u_1, \tag{34c}$$

$$-\mathrm{i}\omega g_1=\beta' u_1-\gamma_{\mathrm{LD}}g_1-\mathrm{i}q_r g_1, \tag{34d}$$

where n_2^* is the complex conjugate of n_2. Now we assume an ordering as $n_0,u_1,g_1\sim O(1)$, $n_2\sim O(\epsilon)$. From Eqs. (34c) and (34d), we first obtain the relation,

$$-\mathrm{i}(\omega-q_r v_{\mathrm{gr,GAM}})-\frac{\alpha'}{2}n_0+\omega_{\mathrm{GAM}}^2\frac{1}{-\mathrm{i}(\omega-q_r v_{\mathrm{gr,GAM}})+\gamma_{\mathrm{LD}}}=0. \tag{35}$$

Due to the condition that n_0 must be real, we obtain the following dispersion relation for ω:

$$(\omega-q_r v_{\mathrm{gr,GAM}})\{[(\omega-q_r v_{\mathrm{gr,GAM}})^2+\gamma_{\mathrm{LD}}^2]-\omega_{\mathrm{GAM}}^2\}=0. \tag{36}$$

Thus, we find

$$\omega=q_r v_{\mathrm{gr,GAM}},q_r v_{\mathrm{gr,GAM}}\pm\sqrt{\omega_{\mathrm{GAM}}^2-\gamma_{\mathrm{LD}}^2}. \tag{37}$$

Substituting $\omega-q_rV_{\mathrm{gr,GAM}}=\sqrt{\omega_{\mathrm{GAM}}^2-\gamma_{\mathrm{LD}}^2}$ into Eq. (35) to lowest order, we obtain

$$\left(\frac{\alpha'}{2}n_0-\gamma_{\mathrm{LD}}\right)u_1=0, \tag{38}$$

$$n_0=\frac{2\gamma_{\mathrm{LD}}}{\alpha'}=N_*,$$

$$n_0(\gamma_L-\Delta\omega n_0-\alpha'|u_1|^2)=0, \tag{39}$$

$$|u_1|^2=\frac{\Delta\omega}{\alpha'}(N_L-N_*).$$

Because $|u_1|^2$ in Eq. (39) must be positive, we find that $N_L>N_*$ is necessary for the limit-cycle solution to exist.

We can estimate the critical scaling of the input of heating power characterized by γ_L, as $|u_1|^2\propto(\gamma_L-\gamma_{L,\mathrm{crit}})$, which is consistent with the result in the parameter scan of γ_L as seen in Fig. 3(b).

We can find the mechanisms for transition from an L-modelike stationary state to GAM limit-cycle state by increasing the power heating γ_L. In the low heating power regime, where γ_L is low, L-modelike confinement occurs, in which the turbulence level is simply proportional to γ_L as in usual mixing length and quasilinear estimates. As heating power increases, the L-modelike turbulence level N_L becomes higher than N_* and N_H, thus indicating a possible change to one of these as a state of higher confinement. Figure 4 illustrates the transition process from the L-modelike state to the GAM oscillatory one by increasing the power heating.

From these results, a diagram of the state of turbulence as a function of $(\gamma_L,\gamma_{\mathrm{LD}})$ for fixed ω_{GAM} and the other parameters is shown in Fig. 5. It shows that, given a set of parameters, system will converge to the state with a certain turbulence level determined by the minimum of the three characterized variables, i.e., (i) L-modelike steady state N_L, (ii) reduced turbulence steady state N_H, and (iii) oscillatory GAM state N_*. Therefore by comparing any two of its val-

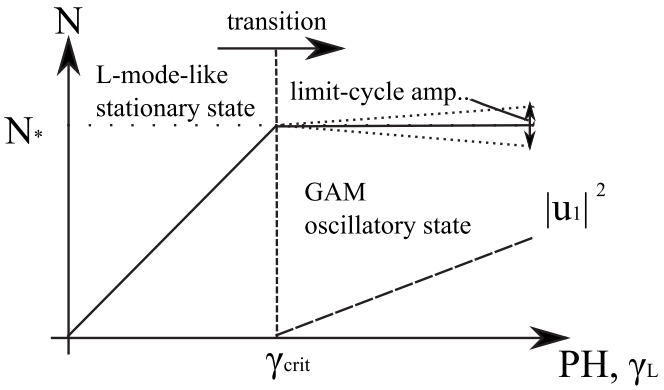

FIG. 4. Illustration of the transition from an L-modelike stationary state (left) to an limit-cycle GAM state (right) by increasing heating power or γ_L.

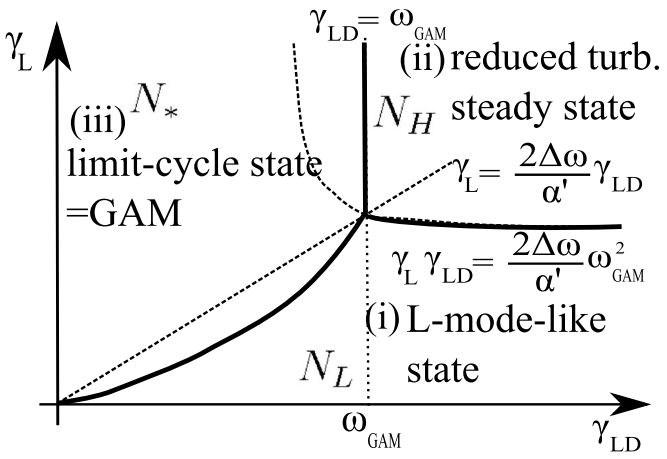

FIG. 5. Diagram of the turbulence convergence in (γ_L, γ_{LD}). The turbulence level is determined by the minimum one of the three states: (i) L-modelike state with the turbulence level $N=N_L$, (ii) reduced turbulence steady state with $N=N_H$, and (iii) limit-cycle GAM state with $N=N_*$. Bold lines show the critical boundary between two states.

ues, we can find the marginality condition in parameter space. Between N_L and N_H, marginality is defined by

$$\gamma_L \gamma_{\mathrm{LD}} = \frac{2\Delta\omega}{\alpha'}\omega_{\mathrm{GAM}}^2. \tag{40a}$$

Marginality between N_L and N_* and between N_H and N_* are defined, respectively, by

$$\gamma_L = \frac{2\Delta\omega}{\alpha'_{\mathrm{eff}}}\gamma_{\mathrm{LD}}, \tag{40b}$$

$$\gamma_{\mathrm{LD}} = \omega_{\mathrm{GAM}}, \tag{40c}$$

where α'_{eff} is the parameter α' modified by the effect of finite real frequency, which is calculated later including the effect of the radiative dissipation. It is found that with lower heating power, γ_L tends to the L-modelike stationary state, where turbulence saturates at the level N_L, and U and G are damped. On the other hand, above a certain critical heating power, turbulence tends to the high confinement state, where it is oscillatory when γ_{LD} is sufficiently weak as compared with the GAM frequency ω_{GAM}. When the Landau damping time is slower than the GAM time, $\tau_{\mathrm{LD}} < \tau_{\mathrm{GAM}}$, the oscillatory state will stop and an reduced turbulence steady state is established. Note that inclusion of a contribution from the ZFZF or mean flow is necessary to accurately reproduce an H-mode state in this model, since the peak at the GAM frequency disappears in the observed H-mode state. Therefore inclusion of the contribution of $\langle v_{\|} \cos\theta \rangle$ is needed to reproduce a transition from a GAM limit-cycle state to the H-mode state, because zero-frequency eigenmodes are not excited when $\gamma_{\mathrm{LD}} < \omega_{\mathrm{GAM}}$.

Next we will identify the eigenfrequency of the GAM in the case that it is the limit-cycle state, which is modified by the effect of GAM group propagation as well as Landau damping. We obtain the modified profile of the GAM frequency ω as a function of q_r incorporating propagation effects as well as polarization effects. Including the effect of ion polarization screening effects, the GAM frequency has a dependency on q_r, i.e., $\omega_{\mathrm{GAM}} \propto (1+q_r^2)^{-1/2}$. As seen in Eq. (37), the effective GAM frequency, (that is the laboratory frame frequency), involves the group velocity, $v_{\mathrm{gr,GAM}} = \partial\omega/\partial q_r$. Therefore solving these as differential equations for $\omega(q_r)$, we can find the explicit description of the GAM frequency including the radiative dissipation as well as the polarization screening. Now we have two candidates,

$$\omega = q_r \frac{\partial\omega}{\partial q_r}, \tag{41a}$$

$$\omega = q_r \frac{\partial\omega}{\partial q_r} \pm \sqrt{\omega_{\mathrm{GAM}}^2 - \gamma_{\mathrm{LD}}^2}. \tag{41b}$$

First we solve Eq. (41a). The solution is the form of $\omega = A q_r$, where A is an integral constant determined by the boundary condition. From the boundary condition that $\omega(q_r)$ must be finite in the limit of $q_r \to \infty$, $A=0$ is found, so $\omega=0$, which corresponds to a stationary case, without propagation.

In solving Eq. (41b), we need keep in mind of the dependence of ω_{GAM} on q_r and consider the case without γ_{LD} as a simple case. ω is shown to be

$$\begin{aligned}\omega &= q_r\left(\int \frac{1}{q_r^2}\frac{\omega_{\mathrm{GAM},0}}{\sqrt{1+q_r^2}}\mathrm{d}q_r + C\right),\\ &= \sqrt{1+q_r^2}\,\omega_{\mathrm{GAM},0} + q_r C,\end{aligned} \tag{42}$$

where C is an integral constant. We need to set $C = -\omega_{\mathrm{GAM},0}$ due to the condition that $\omega \to 0$ is satisfied when $q_r \to \infty$. Finally, we obtain

$$\begin{aligned}\omega &= \omega_{\mathrm{GAM},0}(\sqrt{1+q_r^2} - q_r)\\ &= \omega_{\mathrm{GAM},0}\frac{(\sqrt{1+q_r^2}-q_r)(\sqrt{1+q_r^2}+q_r)}{\sqrt{1+q_r^2}+q_r}\\ &= \frac{\omega_{\mathrm{GAM},0}}{q_r + \sqrt{1+q_r^2}}.\end{aligned} \tag{43}$$

Notice that we obtain the factor $1/(q_r + \sqrt{1+q_r^2})$ from the effect of the radiative dissipation, instead of the factor of

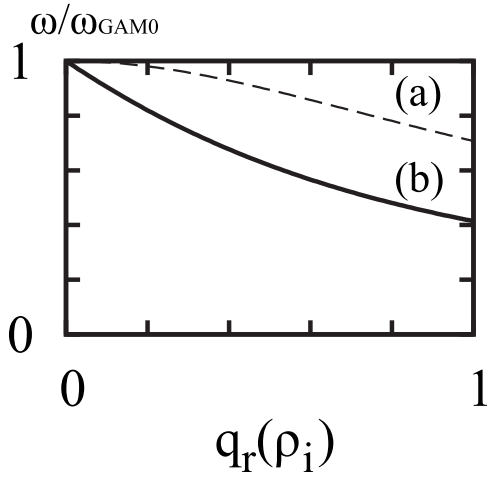

FIG. 6. The evolution of the GAM frequency ω as a function of q_r in the case (a) without propagation and (b) with propagation.

$1/\sqrt{1+q_r^2}$ in the case without radiative dissipation.

Figure 6 shows the evolution of the GAM frequency ω as a function of q_r in the cases (a) without and (b) with GAM propagation. We see that including the effect of GAM propagation reduces the effective frequency from $1/\sqrt{1+q_r^2}$ to $1/(q_r+\sqrt{1+q_r^2})$, as illustrated in Fig. 6.

Next we solve the case with finite γ_{LD}. We see that

$$\omega = \omega_{\mathrm{GAM},0} q_r \left(\int \frac{1}{q_r^2} \sqrt{\frac{1}{1+q_r^2} - a^2} \mathrm{d}q_r + C \right), \tag{44}$$

where $a=\gamma_{\mathrm{LD}}/\omega_{\mathrm{GAM},0}$. Through lengthy calculation, we finally obtain

$$\frac{\omega}{\omega_{\mathrm{GAM},0}} = a q_r \left\{ E\left[\sinh^{-1}\left(\sqrt{\frac{a^2}{1-a^2}} q_r \right) \middle| 1 - \frac{1}{a^2} \right] \right\} + \sqrt{1+q_r^2}\sqrt{1-a^2(1+q_r^2)} - q_r, \tag{45}$$

where $E(\phi|m)$ is the elliptic function of the second kind. Figure 7 shows the evolution of $\omega/\omega_{\mathrm{GAM},0}$ as a function of q_r and γ_{LD}.

Here we discuss the effect of the Doppler effect of the GAM propagation on turbulence transport. Because of the Doppler effect, the effective GAM frequency decreases, so the autocorrelation time scale $\tau_{\mathrm{ac,GAM}}$ is also reduced. Thus the steady state level of turbulence N_* is also reduced. The total estimated level of turbulence governed by the GAM is determined by the relation among the GAM frequency, the turbulence group velocity, and the effect of GAM propagation.

IV. CONCLUSION AND REMARKS

We have analyzed the impact of the GAM on turbulence and transition. First we have discussed the effect of its real frequency on ZF modulation. Because of the change in the resonance conditions, secular shearing due to the GAM frequency occurs and a new time scale, namely, the wave packet-GAM autocorrelation time, is defined. Its variation follows from a comparison between the scale of the GAM

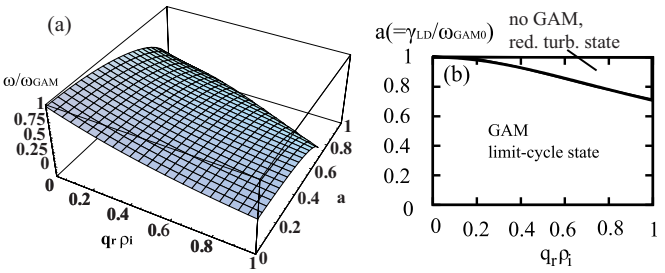

FIG. 7. (Color online) (a) The evolution of the GAM frequency $\omega/\omega_{\mathrm{GAM},0}$ including the effect of the radiative dissipation as a function of q_r and $a(=\gamma_{\mathrm{LD}}/\omega_{\mathrm{GAM},0})$. Note that the GAM can be established only in the region $\gamma_{\mathrm{LD}} < 1/\sqrt{1+q_r^2}$, as shown in (b).

frequency and that of the diamagnetic drift frequency. The ratio is approximately comparable to $(1+a/R)$.

As compared to the previous work for the estimation of the time-evolving $\mathbf{E}\times\mathbf{B}$ shearing rate,[15] we have formulated a more complete calculation of the rate of generation of the ZF with real frequency and how it depends on the spectrum of turbulence. We identify the process of secular stochastic shearing, in which drift wave packets resonate with the dispersive GAM shearing field. Our result somewhat resembles Hahm's, in that the change in ZF modulation is the order of the ratio of real frequency of the GAM to the GAM field autocorrelation rate. However, the autocorrelation rate can be larger than frequency, due to modest GAM dispersion.

We have also examined the effects of GAM group propagation. The effect produces both nonlocality of turbulence as well as radiative dissipation. Regarding nonlocal turbulence dynamics, the dimensionless scale length of radial propagation can be defined as the ratio of GAM frequency ω_{GAM} to the Landau damping γ_{LD}, which may be large in the large $q(r)$ edge region. This indicates that nonlocal edge-core coupling dynamics may involve such GAM propagation, so that the GAMs can play a role in bursty phenomena of turbulence in the edge region. This also defines a new edge length scale.

To discuss the effect of the GAMs on turbulence, we construct the zero-dimensional predator-prey model which relates turbulence and the GAM components. The parameters governing the system are the following four variables: The growth rate can be classified into that of the nonlocal turbulence fluctuation γ_L, which is determined by heating power and by the net incremental temperature gradient relative to a critical gradient. The Landau damping rate of the GAM γ_{LD} is determined by wave-particle resonance,[23] and has a strong dependency on $q(r)$. When we consider a high $q(r)$ value, the Landau damping rate is weak. The ZF modulation rate α' is determined by a modulational analysis using the wavekinetic equations, and is related to the spectrum of turbulence, $\partial\langle N\rangle/\partial k_r$, and also the real frequency of the GAMs. Considering the stationary state, we treat it as we do the state with ZFZFs. While when discussing the limit-cycle state, we use the parameter incorporating the secular shearing effect including the real frequency. The reference GAM frequency ω_{GAM} is determined by the fluid estimation, but it can also be generalized and obtained from a gyrokinetic analysis. We

take into account the q_r dependency of the FLR or ion polarization screening effect.

The stability analyses around fixed points reveal three kinds of states: (i) an L-modelike stationary state, (ii) a reduced turbulence stationary state, and (iii) a limit-cycle GAM state. We find that the system is attracted to the state with the lowest turbulence level of the three.

Solving the eigenvalue equation and the corresponding differential equation in terms of radial wave number q_r, we find the effective GAM frequency incorporating the effect of the radiative dissipation, as well as Landau damping and ion polarization screening effect. Due to the radiative dissipation, the GAM frequency is found to be downshifted by the GAM radiative Doppler effect. Due to the Doppler effect, the steady level of the turbulence is suppressed by the effective reduction in the GAM frequency.

The reduction in the GAM frequency due to the radiative dissipation may explain the difference between theoretically predicted and experimentally observed GAM frequencies. As seen in Fig. 2 in Ref. 14, the observed GAM frequency from the Landau-fluid simulation is seen to be below the theoretically predicted profile f_{GAM}. In Miyato's simulations, the radial wave number $q_r\rho_i \sim 0.3$ is calculated from the estimation of the bandwidth of the GAM islands Δr, which implies about a 25% reduction in the frequency. This reduction factor is consistent with the result of the simulations.

An interesting question here is to discuss the implications of the radiative dissipation for conventional gyrokinetic theory or radial eigenmode theory. The calculation of radiative dissipation is quite general and may be applied to other models by using Eq. (15). These investigations are still under consideration and will be discussed in future work.

One remark concerns the possibility of return of energy from the GAM to the drift wave turbulence, as discussed in Refs. 21 and 24. In our work, such an effect is not treated, for simplicity. In the present study, we find turbulence backflow cannot be reproduced. However, we note that when $\phi(1,0)$, a sideband of the GAM, is excited, the convective term associated with $\phi(1,0)$ becomes non-negligible. This is qualitatively different dynamics from the effect of GAM propagation, which is based on finite frequency. Due to the convection by $\phi(1,0)$, the excitation of $\phi(m\pm 1,n)$ may be enhanced, followed by turbulence spreading. If it is true, edge turbulence need not be directly excited by "GAM backflow," but rather by indirect enhancement through spatial coupling mediated by the GAM. A detailed analysis will be presented in future work.

The theory of the Doppler effect of the GAM frequency applies not only to the fluid regime, but also to the kinetic one. In many simulation results, the observed GAM frequency in the steady state regime does not agree with the theoretical one. We suggest that the mismatch occurs not only due to the formation of coherent radial eigenmodes but also due to the Doppler dissipative effect.

ACKNOWLEDGMENTS

The authors would like to thank Z. Lin, Y. Xiao, T. S. Hahm, J. Q. Li, K. Itoh, C. S. Chang, M. Malkov, and N. Miyato for helpful suggestions and discussion on this work. We also acknowledge stimulating discussions of experimental results with G. Conway, J. Dong, G. McKee, and G. Tynan.

This work is supported by the Department of Energy under Award Nos. DE-FG02-04ER54738 and DE-FC02-08ER54959.

[1] P. H. Diamond, S.-I. Itoh, K. Itoh, and T. S. Hahm, Plasma Phys. Controlled Fusion **47**, R35 (2005).
[2] M. N. Rosenbluth and F. L. Hinton, Phys. Rev. Lett. **80**, 724 (1998).
[3] N. Winsor, J. L. Johnson, and J. M. Dawson, Phys. Fluids **11**, 2448 (1968).
[4] A. Fujisawa, A. Shimizu, H. Nakano, S. Ohshima, K. Itoh, Y. Nagashima, S.-I. Itoh, H. Iguchi, Y. Yoshimura, T. Minami, K. Nagaoka, C. Takahashi, M. Kojima, S. Nishimura, M. Isobe, C. Suzuki, T. Akiyama, T. Ido, K. Matsuoka, S. Okamura, and P. H. Diamond, J. Phys. Soc. Jpn. **76**, 033501 (2007).
[5] G. R. McKee, P. Gohil, D. J. Schlossberg, J. A. Boedo, K. H. Burrell, J. S. deGrassie, R. J. Groebner, M. A. Makowski, R. A. Moyer, C. C. Petty, T. L. Rhodes, L. Schmitz, M. W. Shafer, W. M. Solomon, M. Umansky, G. Wang, A. E. White, and X. Xu, Proceedings of the 22nd IAEA Fusion Energy Conference, Geneva, Switzerland, 2008.
[6] G. D. Conway, E. Poli, T. Happel, and ASDEX Upgrade Team, Proceedings of the 19th International Toki Conference, Toki, Japan, 2009.
[7] J. Q. Dong, K. J. Zhao, L. W. Yan, W. Y. Hong, C. X. Yu, A. Fujisawa, L. H. Yao, J. Qian, J. Cheng, A. D. Liu, T. Lan, H. L. Zhao, D. F. Kong, Y. Liu, Y. Huang, Q. Li, X. M. Song, Q. W. Yang, X. T. Ding, X. R. Duan, and Y. Liu, Proceedings of the 19th International Toki Conference, Toki, Japan, 2009.
[8] K. Itoh, S.-I. Itoh, P. H. Diamond, A. Fujisawa, M. Yagi, T. Watari, Y. Nagashima, and A. Fukuyama, Plasma and Fusion Research **1**, 037 (2006).
[9] Z. Lin and T. S. Hahm, Phys. Plasmas **11**, 1099 (2004).
[10] T. S. Hahm, P. H. Diamond, Z. Lin, G. Rewoldt, O. Gurcan, and S. Ethier, Phys. Plasmas **12**, 090903 (2005).
[11] M. A. Malkov, P. H. Diamond, and M. N. Rosenbluth, Phys. Plasmas **8**, 5073 (2001).
[12] A. I. Smolyakov, P. H. Diamond, and M. Malkov, Phys. Rev. Lett. **84**, 491 (2000).
[13] P. H. Diamond, S. Champeaux, and M. Malkov, Nucl. Fusion **41**, 1067 (2001).
[14] N. Miyato, Y. Kishimoto, and J. Q. Li, Plasma Phys. Controlled Fusion **48**, A335 (2006).
[15] T. S. Hahm, M. A. Beer, Z. Lin, W. Hammett, W. W. Lee, and W. M. Tang, Phys. Plasmas **6**, 922 (1999).
[16] Ö. D. Gürcan, P. H. Diamond, T. S. Hahm, and Z. Lin, Phys. Plasmas **12**, 032303 (2005).
[17] K. Miki, Y. Kishimoto, N. Miyato, and J. Q. Li, Phys. Rev. Lett. **99**, 145003 (2007).
[18] K. Miki, Y. Kishimoto, J. Q. Li, and N. Miyato, Phys. Plasmas **15**, 052309 (2008).
[19] K. Miki, Y. Kishimoto, N. Miyato, and J. Q. Li, J. Phys.: Conf. Ser. **123**, 012028 (2008).
[20] M. A. Malkov and P. H. Diamond, Phys. Plasmas **8**, 3996 (2001).
[21] N. Miyato, Y. Kishimoto, and J. Li, Phys. Plasmas **11**, 5557 (2004).
[22] M. W. Hirsch, S. Smale, and R. L. Devaney, *Differential Equations, Dynamical Systems, and an Introduction to Chaos* (Elsevier Academic, New York, 2004).
[23] H. Sugama and T.-H. Watanabe, Phys. Plasmas **13**, 012501 (2006).
[24] K. Hallatschek and D. Biskamp, Phys. Rev. Lett. **86**, 1223 (2001).